Acta Cryst. (1982). A**38**, 695–702

High-Resolution Electron Microscopy of McGillite. II. Polytypism and Disorder

BY SUMIO IIJIMA*

Center for Solid State Science, Arizona State University, Tempe, Arizona 85287, *USA*

(*Received* 15 *September* 1981; *accepted* 19 *April* 1982)

Abstract

A new series of polytypes of a sheet silicate mineral, mcGillite, has been found using high-resolution electron microscopy. Their crystal structures are described in terms of the stacking sequence of the one-layer monoclinic structure [Iijima (1982) *Acta Cryst.* A**38**, 685–694]. Multiplicity of the polytypes results from regular occurrences of the 120° rotation twinning on the basal (001) plane. The two- and three-layer polytypes found in the present study are both monoclinic and are different from two-layer schallerite and three-layer friedelite, belonging to the family of manganpyrosmalite and being reported as trigonal.

1. Introduction

The preceding paper (Iijima, 1982)† dealt with electron optical studies of crystals of a sheet silicate mineral mcGillite from the Sullivan mine, Kimberley, British Columbia, Canada. The mineral has been reported as mcGillite, the fifth member of the pyrosmalite group (Donnay, Betournay & Hamill, 1980). Our examination of this mineral, however, showed that its basic one-layer structure is monoclinic, which is different from the trigonal one-layer structure of manganpyrosmalite (Takéuchi, Kawada & Sadanaga, 1963). Considerable disorder in stacking of SiO_4 tetrahedral sheets and brucite-like $Mn(OH)_2$ octahedral sheets in the c-axis direction was found to be caused by 120° rotation twinning on the (001) plane. The twinning takes place on a very small scale down to a single unit-cell width. High-resolution electron microscope observation on disordered regions of the crystals revealed the nature of such small-scale twinnings.

According to the literature (Donnay, Betournay & Hamill, 1980), manganpyrosmalite $(Mn,Fe)_8(Si_6O_{15})(OH,Cl)_{10}$ has three other forms. Their c axes are multiples of that of the one-layer structure of pyrosmalite. Schallerite, friedellite and mcGillite were reported as having c axes $2c_0$, $3c_0$ and $12c_0$. The first two structures are reported as trigonal (Takéuchi, Kawada, Irimagiri & Sadanaga, 1969). The extreme similarity of their chemical formulae imposes a difficulty in explaining the origin of polytypism of manganpyrosmalite in terms of chemical composition.

The present paper is concerned with polytypism of mcGillite. We found six polytypes, $1\times$, $2\times$, $3\times$, $4\times$, $6\times$ and $9\times c_0$, where $c_0 = c/\sin\beta$, c and β are from the $1M_1$ structure.

2. Specimen and experimental procedure

The crystal of manganpyrosmalite examined here is from the Sullivan mine, Kimberley, Canada and was reported as a new mineral mcGillite (Donnay, Betournay & Hamill, 1980). Its basic crystal structure has been described as monoclinic in paper I.

The specimens for the electron micrscope examination were prepared by grinding the crystals. We assumed that this grinding process would not introduce any structural modification into the original crystal since we have not observed dislocations suggesting mechanical shear on the basal (001) plane, which is the cleavage surface. The crystallites were examined in their [110], [010], and [1$\bar{1}$0] zone-axis settings which are obtained by a double-tilt goniometer stage in the JEOL-100B, JEOL-200CX or Philips-EM400 microscope.

3. Description of stacking sequences

Polytypes in mcGillite result from some regular arrangements of the 120° rotation twinning on (001) planes of the $1M_1$ structure. Stacking disorders of this crystal are due to random occurrences of the twin planes. In this section we introduce literal representation and schematic diagrams of stacking sequences of manganpyrosmalite. We shall follow the expression that was used for describing polytypes of the mica group (Iijima & Buseck, 1978).

* Present address: Research and Development Corporation of Japan, Department of Physics, Meijo University, Yagoto-Urayama, Tenpaku-ku, Nagoya, Japan.

† Hereafter this paper is referred to as paper I.

0567-7394/82/050695-08$01.00

The basic monoclinic unit cell projected onto a (001) plane is reproduced in Fig. 1(*a*). Two adjacent sheets of SiO_4 tetrahedra having a configuration $(Si_6O_{15})^{6-}$ located at $z = 0$ and $z = 1$ are represented by dotted lines and solid lines respectively. The stagger between the two sheets resulting in the $1M_1$ structure will be defined by a stacking vector $-\mathbf{a}/12$ shown by the arrow 1, and its two equivalents shown by arrows 2 and 3. Among theoretically possible stacking vectors connecting the center of the hexagon and small solid dots, we recognized only the two types $-\mathbf{a}/12$ and its equivalents, and $\mathbf{a}/6$ and its equivalents, indicated by 4, 5 and 6. Therefore, we consider below stacking sequences of layers due to these two vectors.

For simplicity, we represent the one-layer monoclinic cell by a hexagon shown in Fig. 1(*b*) which corresponds to a 12-membered ring of the SiO_4 tetrahedral sheet at $z = 0$. Furthermore, we introduce symbols defining single-layer positions referred to the standard single-layer orientation *C* with **a** directed to the left and **b** down. The tetrahedral sheet has point symmetry $\bar{3}m$, so that unlike $\bar{6}mm$ of the interlayer of mica stacking there are only three equivalent positions as shown by *C*, *A* and *B*. For the **a**/6-type stacking vectors, the corresponding layer positions are represented by *X*, *Y* and *Z*. A rotation angle between adjacent tetrahedral sheets within a (001) plane can be found from Fig. 1(*c*), in which the numbers 1, 2 and 3 represent rotation angles +60, +120 and 180° counterclockwise respectively. The negative sign means clockwise rotation with respect to the standard *C* layer.

Using these symbols, a regular sequence of the $1M_1$ structure can be expressed as shown in Fig. 2(*a*), which is written literally [000] (*CCCC*). Similarly the 120° rotation twinning on the (001) plane can be expressed as illustrated in Fig. 2(*b*), with a literal expression $[00\bar{2}00]$ (*CCCBBB*). A high-resolution microscope image of such a twinning has been shown in Fig. 4 of paper I and also will be shown in the present paper.

Another example of the twinning is illustrated in Fig. 2(*c*). A sequence of layers is written as $[0\bar{2}20]$ (*CCBCC*). The twin planes occur successively in two adjacent layers between *C* and *B* layers, and *B* and *C* layers. The second twinning results from a 120° rotation in a counterclockwise direction (see rotation symbol 2). Consequently the monoclinic structures on both sides of the double twin planes remain in the same orientation. This type of double or paired twin has often been observed in our crystal and its high-resolution electron micrographs were shown in Figs. 3 and 6 of paper I.

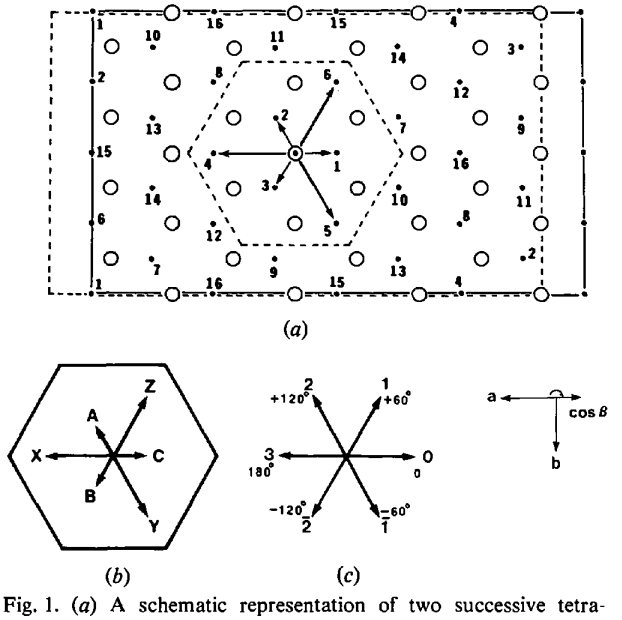

Fig. 1. (*a*) A schematic representation of two successive tetrahedral layers in the monoclinic structure of mcGillite. The dotted lines and solid lines outline the unit cell projected along [001] at $z = 0$ and $z = 1$ respectively. The top tetrahedral sheet is shifted by $-\mathbf{a}/12$ with respect to the bottom one. The hexagon represents a 12-membered ring of SiO_4 in the tetrahedral sheet. Open circles represent positions of OH ions on the $Mn(OH)_2$ octahedral sheet. Vectors connecting the center of the hexagon and small dots depict possible stacking vectors between two successive tetrahedral sheets. (*b*) Designation of six single-layer position symbols, referred to the standard layer orientation *C* with **a** directed to the left and **b** down. (*c*) Vector stacking symbols defining stacking angles between adjacent layers.

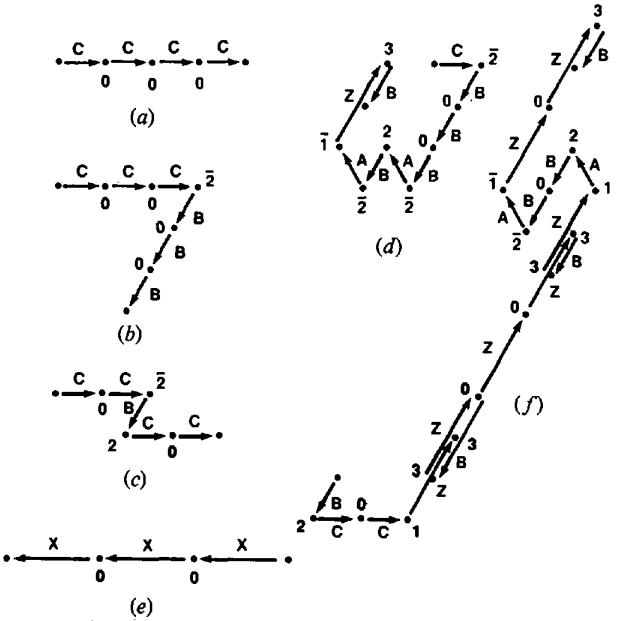

Fig. 2. Diagrammatic representation of stacking vectors in various sequences of mcGillite layers using symbols introduced in Fig. 1. (*a*) A $1M_1$ single-layer monoclinic structure. (*b*) A twinning in the $1M_1$ structure. (*c*) A double-twinning occurring at both sides of the layer in the $1M_1$ structure. (*d*) The stacking sequence of a disordered region of mcGillite derived from a high-resolution structure image of Fig. 3. (*e*) A $1M_2$ single-layer monoclinic structure. Note that the stacking vector is twice as large as that of $1M_1$. (*f*) The stacking sequence of a disordered region of mcGillite derived from a high-resolution image of Fig. 5. The region contains the $1M_2$ monoclinic structure, which is symbolically expressed as [00][*ZZZ*].

Let us consider a more general case of disordered stacking sequences. First we shall establish a procedure to determine positions of individual layers relative to the C position from high-resolution micrographs of mcGillite. Fig. 3 shows a structure image* of a disordered region of the crystal viewed along the **a** direction, $[\bar{1}30]$ or $[1\bar{3}0]$. The dark continuous lines in the horizontal direction correspond to the $Mn(OH)_2$ octahedral sheets. Grey rods appearing between the dark lines represent groups of SiO_4 tetrahedra centred on a mirror plane of the tetrahedral sheet {see the [100] projection of Fig. 1(*d*) of paper I}.

The arrangements of the rods, determined by stacking vectors or the 120° rotation twinning between adjacent layers, are schematically illustrated by black dots on the left-hand side of the micrograph. Four different types of arrangement are recognized when going from one layer to its neighboring ones such as across layer 1, layers 2, 3, 4, 6 and 9, layers 5 and 7, and layer 8. Angles between a line connecting two adjacent dots and the b axis are 90, +75, −75 or 65°. The first three angles correspond to those between b and c axes of the $1M_1$ structure projected along [100], $[\bar{1}30]$ and $[1\bar{3}0]$ respectively. If we take the position of layer 1 as a standard C, the sequence of layers is designated as *CBBBABAZB*, which is shown at the right-hand side of the micrograph.

* It has been experimentally and theoretically shown that image intensities of high-resolution lattice images of very thin crystals, say less than 50 Å thick, recorded under the condition of 'optimum focus' of the objective lens are roughly proportional to projected crystal potentials along the incident beam direction. Therefore such images reveal the arrangement of relatively heavy atoms in crystals (O'Keefe, Buseck & Iijima, 1978).

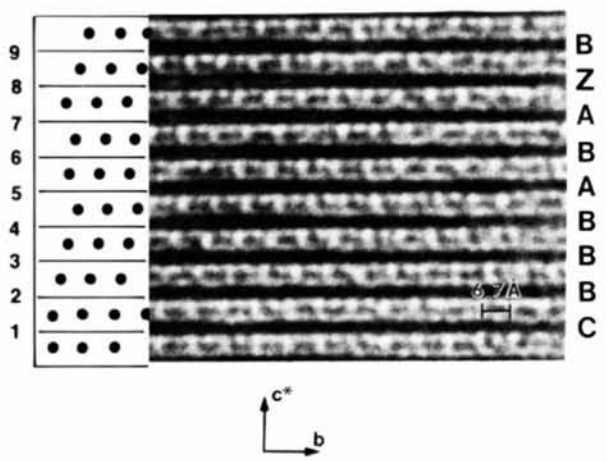

Fig. 3. A high-resolution structure image showing a (100) plane projection of a mcGillite crystal. The darkest continuous lines in the horizontal direction correspond to the individual $Mn(OH)_2$ octahedral sheets. Rods between the octahedral sheets represent tetrahedral sheets. A stacking sequence of layers 1 to 10 has been analyzed as shown in Fig. 2(*d*).

The arrangement of the black dots at layer 8 is such that the dots on both sides of the layer are shifted mutually by a distance **b**/4, and the others by 0, or $\pm$**b**/8. The position of this layer is designated as Z in Fig. 1(*b*), which is associated with the second set of stacking vectors shown by the arrows 4, 5 and 6 in Fig. 1(*a*). A regular stacking of this layer will result in a new type of single-layer monoclinic structure, which will be discussed in §4.

A stacking sequence of the layers from 1 to 9 shown in Fig. 3 is therefore written as $[\bar{2}00\bar{2}2\bar{1}3]$ (*CBBBABAZB*). Its diagram is illustrated in Fig. 2(*d*). It is seen that a region from layer 2 to layer 4 forms locally the $1M_1$ structure. A sequence of $[\bar{2}2\bar{2}]$ (*BABA*) might be considered as a polytype having a doubled c axis, which actually has been found in mcGillite and will be shown in a later section.

4. Single-layer monoclinic structure $1M_2$

A regular arrangement of the layers with a stacking vector **a**/6 (arrow 4 in Fig. 1*a*) will lead to a single-layer polytype of mcGillite. The structure becomes monoclinic (Fig. 2*e*). We call it $1M_2$ hereafter. Its literal expression is $1M_2[0](X)$. Fig. 4 illustrates an idealized model for the $1M_2$ structure projected along [010]. The monoclinic angle β becomes theoretically 118·6°. The other lattice parameters are $a = 23{\cdot}397$, $b = 13{\cdot}489$, $c = 8{\cdot}132$ Å with space group $C2/m$.

Fig. 5 reproduces a high-resolution electron micrograph of a disordered region of the crystal in the same orientation as that of Fig. 3. The image intensity however has been modified by a dynamical diffraction effect of the electron waves because the crystal was too thick. Nevertheless we noticed that white dots in the micrograph appear at regions between adjacent grey dots shown in Fig. 3. This will be sufficient for defining positions of the individual layers. By knowing the types of layers (indicated at the top of the micrograph), we analyzed the stacking sequence in the region arrowed. The result is shown in Fig. 2(*f*). The layer Z occurs singly or as groups in some regions.

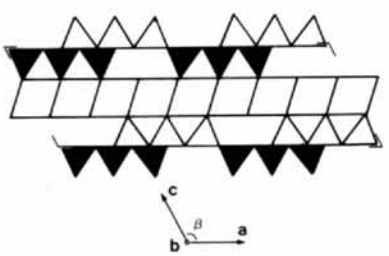

Fig. 4. A model for the $1M_2$ monoclinic structure projected onto the (010) plane. Triangles and parallelograms represent SiO_4 tetrahedra and $Mn(OH)_2$ octahedra respectively.

A region near the center of the micrograph has an arrangement [00](*ZZZ*), which is equivalent to $1M_2$[0](*X*) shown in Fig. 2(*e*). Although the region has only three-unit-cell width, it proves the occurrence of the $1M_2$ structure. The uncommonness of the structure compared with the $1M_1$ in mcGillite would suggest that the two adjacent tetrahedral sheets could interact with each other across the octahedral sheet. Such an interaction should act so that the stacking of the **a**/12 type is energetically favored over that of the **a**/6 type.

5. Polytypism of mcGillite

Two-layer polytypes

Fig. 6(*a*) represents an electron diffraction pattern showing a *h*0*l* reciprocal-lattice section of $1M_1$. Some of its *h*00 spots are indicated by black arrows. The pattern displays another set of spots (some indicated by white arrows). It is seen that for the second type of spots c^* is halved. These spots do not appear for $h = 0$.

For a two-layer structure resulting from the stacking vector 1 of Fig. 1(*a*), only one ordered sequence is theoretically possible. This is illustrated in Fig. 7(*a*), which is symbolically written as $2M[2\bar{2}](CA)$. The structure becomes monoclinic with the lattice parameters $a = 23{\cdot}38$, $b = 13{\cdot}498$, $c = 14{\cdot}4$ Å, $\beta = 97{\cdot}7°$. An oblique angle 86° measured from the pattern of Fig. 6(*a*) agrees quite well with a theoretical value of 86·1° for the postulated structure 2*M* projected along [110].

A structure image corresponding to the electron diffraction pattern of Fig. 6(*a*) will confirm the validity of the 2*M* structure (Fig. 8). Lines of the darkest blobs in the horizontal direction represent the $Mn(OH)_2$ octahedral sheets. Double rows consisting of white blobs appearing between the octahedral sheets correspond to the SiO_4 tetrahedral sheets. There are two types of displacements of the tetrahedral sheets with respect to the position of the octahedral sheets. One is described by a vector $-\mathbf{b}/12$ and thus the displaced portions (arrowed) are exactly the same as a [010] projection of the $1M_1$ structure (see Fig. 7*a* of paper I). The second type of displacement of the tetrahedral sheets has a vector **b**/16. Therefore this arrangement of the sheets becomes identical with the one observed in the image of [110] projection of the $1M_1$ stucture. The unit cell projected along $[\bar{1}10]$ is outlined in the micrograph. Consequently the image will be consistent with the two-layer 2*M* monoclinic structure of Fig. 7(*a*) viewed along the $[0\bar{1}0]$ direction. The structure is different from schallerite which has been reported as trigonal (Bauer & Berman, 1928).

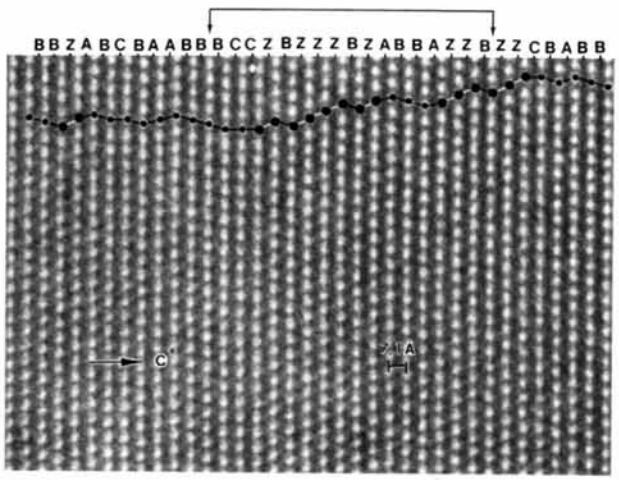

Fig. 5. A high-resolution two-dimensional lattice image of a disordered region of a mcGillite crystal. The stacking sequence in the region between two arrows has been analyzed as shown in Fig. 2(*f*). The stacking sequence indicated by large black dots and white lines results from stacking vectors of **a**/6 and its equivalents. The others are due to $-\mathbf{a}/12$ and its equivalents.

Three-layer polytypes

Fig. 6(*b*) shows an electron diffraction pattern showing a $h\bar{h}l$ reciprocal lattice section. The diffraction spots are streaked slightly parallel to $\mathbf{c}^*$ except for the spots with $h = 4n$. For the spots with $h \neq 4n$, extra peaks appear at the positions with $l = nc^*/3$, suggesting that the *c* axis is tripled. Some of these spots are indicated by white arrows. A high-resolution lattice image taken from a region giving the diffraction pattern of Fig. 6(*b*) is reproduced in Fig. 9. An optical diffraction pattern (inset) taken from the negative of Fig. 9 demonstrates a periodicity of $c^*/3$ similar to the electron diffraction pattern of Fig. 6(*a*).

An inspection of this image revealed a three-layer stacking sequence as illustrated in Fig. 7(*b*). It is symbolically expressed as $3M[02\bar{2}](CCA)$, which contains two successive twin planes. Its unit cell becomes monoclinic with theoretical lattice parameters $a = 13{\cdot}498$, $b = 23{\cdot}379$, $c = 21{\cdot}15$ Å, $\beta = 99{\cdot}0°$. The lattice image shown in Fig. 10 demonstrates a small region of the 3*M* structure oriented with its [310] direction parallel to the incident beam. In this projection, a stacking sequence of three layers is expressed as $3M[02\bar{2}](BAB)$ which is equivalent to the $3M[02\bar{2}](CCA)$.

For three-layer stacking sequences, a trigonal structure designated as $3T[222](CAB)$, space group $P3_112$, is theoretically possible as shown in Fig. 7(*c*). However, we have failed to observe it in our mcGillite. The two structures described here may be compared with a three-layer polytype, friedelite, which is reported as trigonal (Bauer & Berman, 1928). It is of interest to reexamine friedelite in terms of the $1M_1$ structure.

Other multi-layer polytypes

An electron diffraction pattern shown in Fig. 6(*c*) reproduces a 0*kl* reciprocal-lattice section of the $1M_1$

structure. Its $0k0$ spots are indicated by black arrows. As we saw in Fig. 6(b), extra spots (white arrows) appear for the spots $0kl$ with $k \neq 4n$ paralle to the c^* axis. Their positions correspond to $l = nc^*/4$, suggesting that the c axis of this polytype is $4c_0$. An oblique angle between the c^* axis and an axis connecting the spots indicated by white arrows in the near-horizontal direction is measured to be 86·0°.

Fig. 11 reproduces a lattice fringe image of the same crystal as for Fig. 6(c). As indicated in the micrograph, two different polytypes are observed, $4c_0$ and $6c_0$. These polytypes were assigned by measuring their fringe spacings calibrated with the d_{001} spacing of the $1M_1$ structure appearing at the left-hand side of the micrograph.

For a four-layer stacking sequence, four different sequences are possible, as illustrated in Figs. 7(d), (e), (f) and (g). The one shown in Fig. 7(e) is triclinic and the rest of them are monoclinic. They are written as $4M_1|20\bar{2}0|(CCAA)$, $4M_2|2\bar{2}\bar{2}2|(CACB)$, $4M_3|0222|$-$(CCAB)$ and $4\mathrm{Tr}|00\bar{2}2|(CCAC)$. The oblique angle 86·0° measured from the pattern in Fig. 6(c) was found to agree with one expected from the $4M_1$ with lattice parameters a = 23·379, b = 13·498, c = 28·82 Å (= $4c_0 \sin\beta$), β = 97·8°. The structure involves two twin planes occurring at every other layer. Their rotation directions are opposite. The $4M_2$ and $4M_3$ can fit the diffraction pattern of Fig. 6(b) looking down the b axes. Our limited data however have not allowed us to distinguish them.

A six-layer polytype imaged in Fig. 11 has not been analyzed because we failed to observe a high-resolution image of this crystal. It is obvious that as the number of the layers in a polytype is increased, the number of variations in their structures will be increased considerably.

The last example is a polytype consisting of nine layers as shown in Fig. 12(a). We could determine uniquely a stacking sequence by examining a high-resolution lattice image of the polytype (Fig. 12b). This image was taken from an ordered region marked by a dark line in Fig. 12(a). The individual vertical lines are found to be due to a double twinning occurring at both sides of a single layer. The matrix crystal is oriented

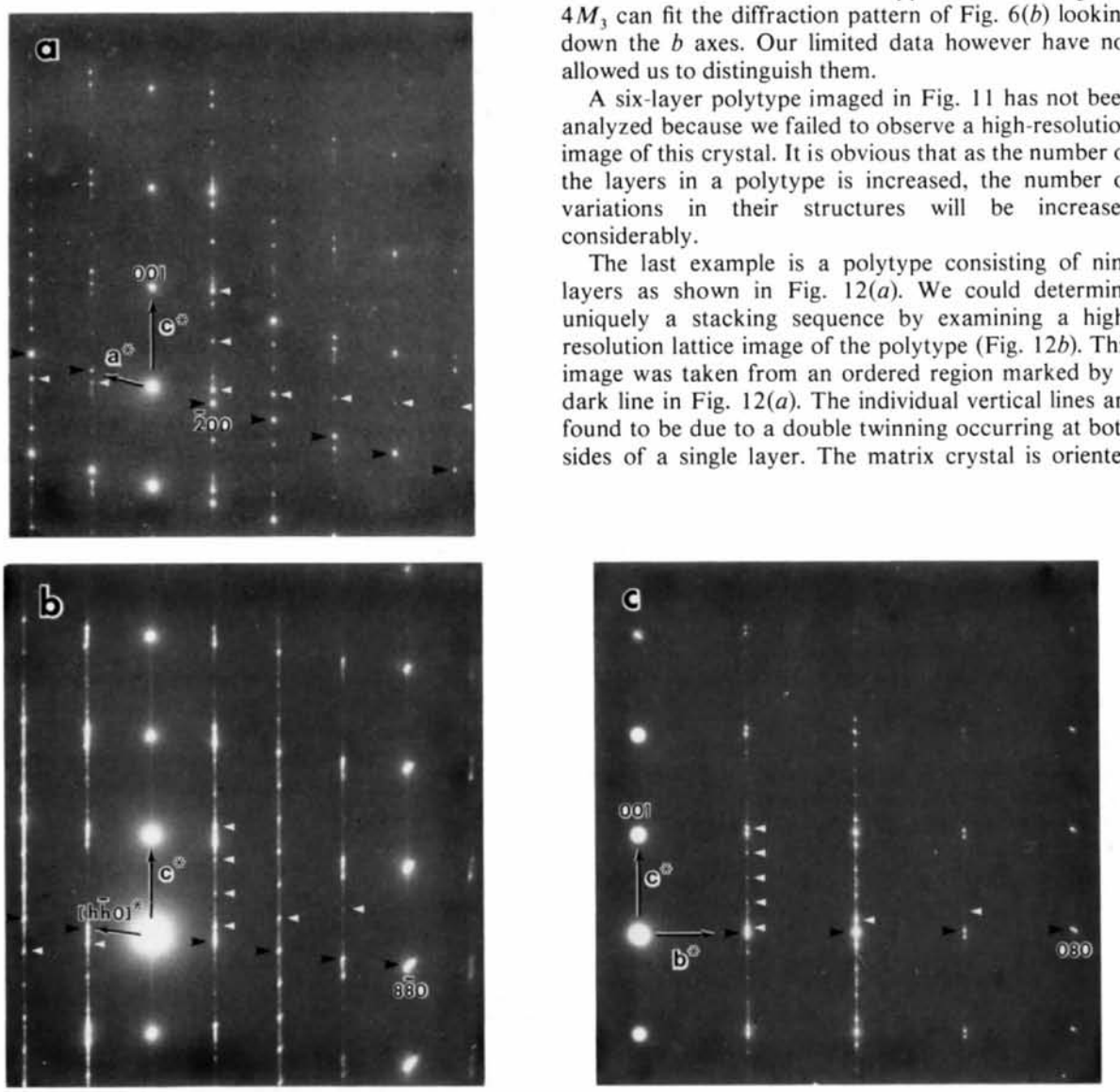

Fig. 6. Electron diffraction patterns of crystals containing polytypes of mcGillite. (a) A $h0l$ reciprocal-lattice section of the $1M_1$ structure, which is superimposed with that of the two-layer polytype of $2M$ structure (indicated by white arrows). (b) A hhl reciprocal-lattice section, which contains the spots due to a three-layer polytype (indicated by white arrows). (c) A $0kl$ reciprocal-lattice section, which contains the spots due to a four-layer polytype (indicated by white arrows).

with its [110] parallel to the incident beam direction. Therefore the lattice fringe system of the d_{001} and d_{100} are inclined to each other by 82° as seen in Fig. 12(*b*). The fringes of the d_{110} make steps at the double twinning (arrowed). It is obvious that the polytype of nine layers results from the regular appearance of a double twinning in a matrix lattice of $1M_1$. The structure therefore can be written as 9Tr[000022000] (*CCCCCACCC*) and it becomes triclinic. Incidentally, a boundary indicated by an arrow in Fig. 12(*a*) is an ordinary twin that has been explained in Fig. 2(*b*).

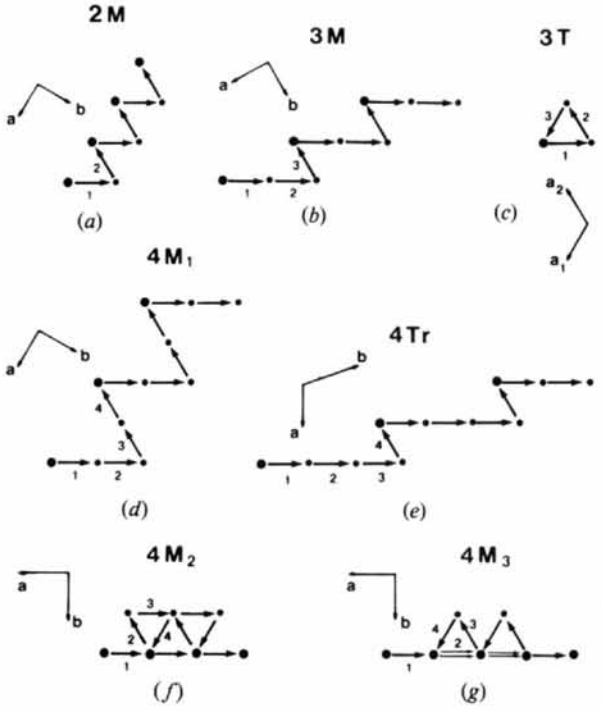

Fig. 7. Diagramatic representations of stacking sequences of polytypes of mcGillite.

Fig. 8. A high-resolution structure image showing a [110] projection of a two-layer polytpe 2*M*. The darkest lines running in the horizontal direction correspond to the $Mn(OH)_2$ sheets. Individual octahedra separated by 2·9 Å are imaged as dark blobs. Arrangements of white blobs corresponding to the tetrahedral sheets are identical at both sides of the octahedral sheets, indicated by arrows, proving the *c* axis to be doubled.

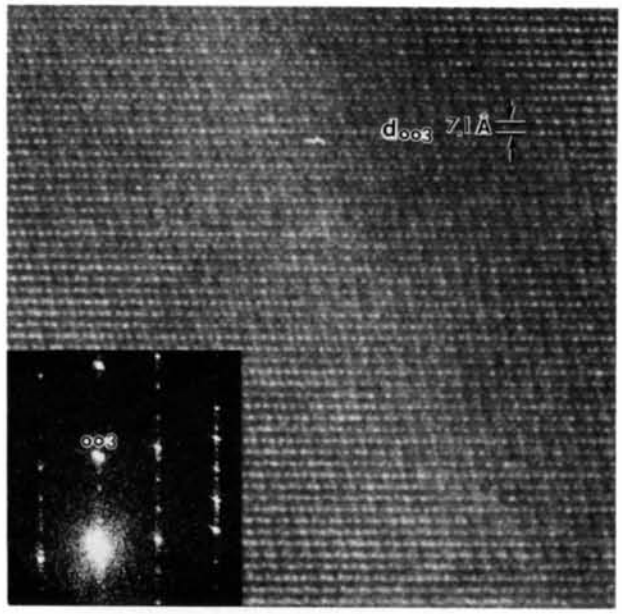

Fig. 9. A high-resolution lattice image from the same crystal as for Fig. 6(*b*), showing a three-layer polytype of mcGillite. Inset demonstrates an optical diffraction pattern of the micrograph, showing **c***/3 spots.

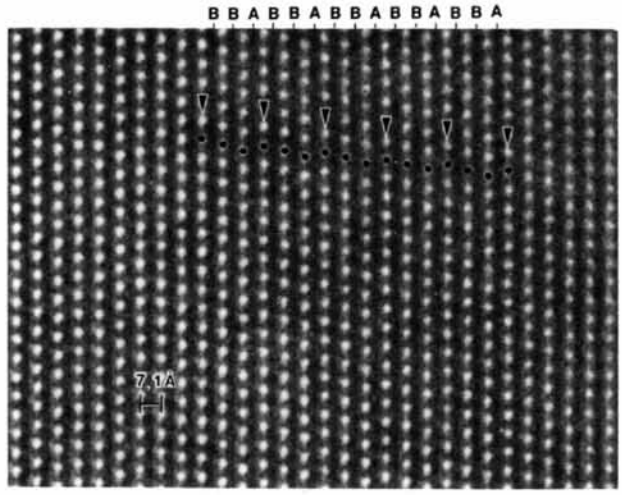

Fig. 10. A high-resolution lattice image image showing a [011] projection of a three-layer polytype. A stacking sequence [02$\bar{2}$] (*BBA*) indicated by arrows is equivalent to that of Fig. 7(*b*).

6. Conclusions

Crystal data of polytypes in mcGillite described in the preceding section are summarized in Table 1. The structures of the polytypes except for $1M_2$ are composed of multiple numbers of layers of the $1M_1$ monoclinic structure. The multiplicity results from occurrences of the 120° rotation twinning on the basal

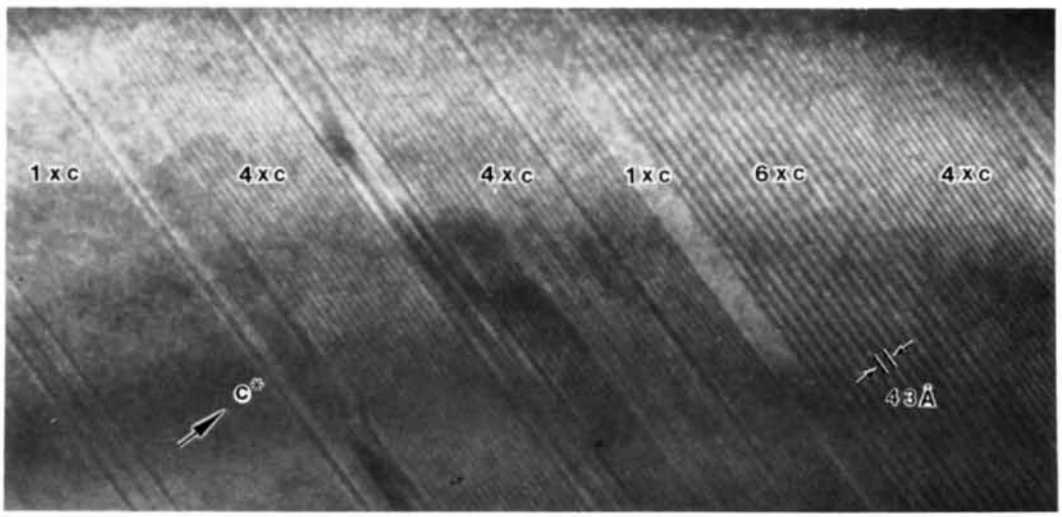

Fig. 11. A one-dimensional lattice image of a [011] projection corresponding to the electron diffraction pattern of Fig. 6(*c*). Two polytypes of four and six layers are imaged. The four-layer polytype is analyzed as that of Fig. 7(*d*).

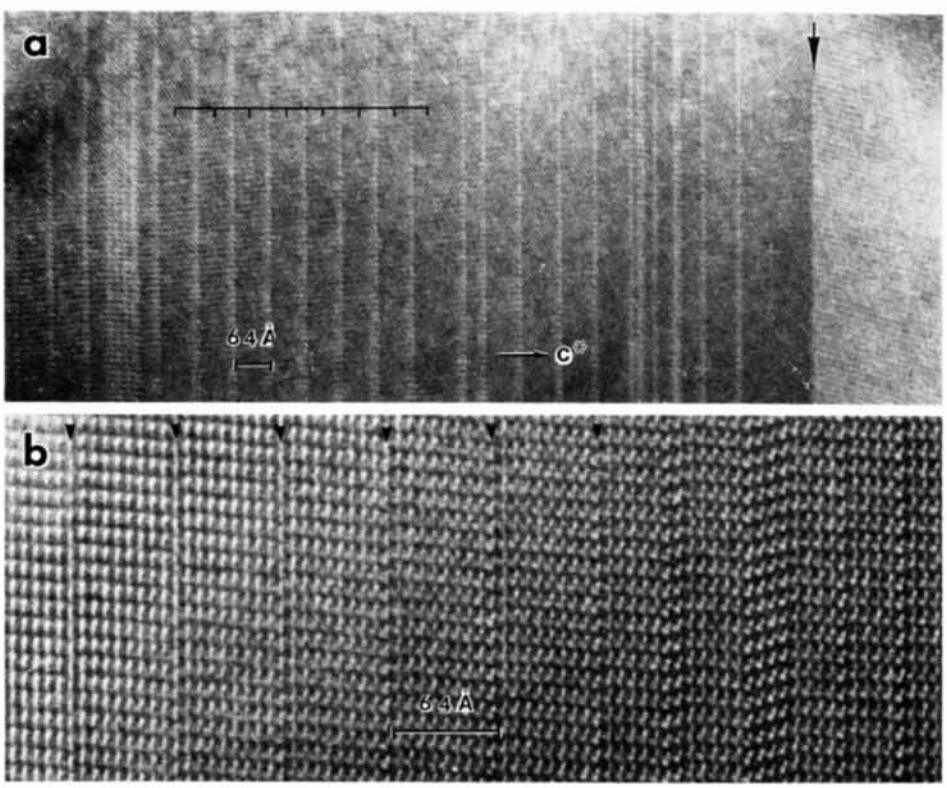

Fig. 12. (*a*) A nine-layer polytype appearing in the small region indicated by a dark line. The boundary marked by an arrow is a (001) twin plane. (*b*) A high-resolution lattice image showing a nine-layer polytype, demonstrating that vertical lines causing the polytype seen in (*a*) are due to a double twinning occurring at both sides of a single layer.

Table 1. *Crystal data of polytypes of mcGillite*

All lattice parameters are calculated by referring to the $1M_1$ structure.

Polytypes underlined have been observed in the present study.

	Space group	Symbols	Unique axis angle β (°)	a (Å)	b (Å)	c (Å)
$1M_1$	$C2/m$	[0](*C*)	105·3	23·279	13·498	7·390
$1M_2$	$C2/m$	[0](*X*)	118·6	23·279	13·498	8·132
$2M$	$C2/c$	[2$\bar{2}$](*CA*)	97·7	23·379	13·498	14·4
$3M$	$C2$	[02$\bar{2}$](*CCA*)	99·0	13·498	23·379	21·15
$3T$	$P3_112$	[222](*CAB*)	–	13·498	–	21·41
$4M_1$	$C2/c$	[2020](*CCAA*)	97·7	23·379	13·498	28·82
$4M_2$	$C2$	[2222](*CACB*)	93·9	23·379	13·498	28·62
$4M_3$	$C2$	[0222](*CCAB*)	93·9	23·379	13·498	28·62
4Tr	$P1$	[0022](*CCAC*)	?	?	?	28·20
6	?	?	?	?	?	42·3
9Tr	$P1$	[00002$\bar{2}$00](*CCCCCACCC*)	–	23·379	13·498	66·51

(001) plane. There are three non-equivalent positions of the layers in the twinning relative to a given reference layer. A combination of non-equivalent positions of the layers results in polytypes of mcGillite.

The fact that chemical compositions of one-layer mcGillite, two-layer schallerite and three-layer friedelite show an extreme similarity according to the literature (Donnay, Betournay & Hamill, 1980) suggests that the origin of the polytypism of mcGillite may not be controlled by chemical composition. Takeda & Ross (1975) proposed that the mica polytypism of $1M$–$2M_1$ biotite does not appear to be related to any chemical difference. An origin of the mica polytype results from constraints produced in a unit talc layer which would control neighboring layers during an initial stage of crystal growth. Their conclusion may be applied to the polytypism of mcGillite.

In many instances of ordered and disordered structures, we noticed that the twinning tends to occur as a pair at both sides of a single layer. It is noted that their rotation directions are opposite. Such a tendency would be explained by the fact that occurrence of a single twin plane generates constraints around it and they would have been cancelled out by having another twin plane that has an opposite sign.

The constraint could be extended more easily to adjacent layers in mcGillite than in mica layers since the bonding between the tetrahedral layer and octahedral layer is much stronger than an ionic bonding in the mica interlayer. The constraints generated at the twin boundaries would favor frequent occurrence of $1M_1$ over $1M_2$ in mcGillite.

Formation of very long c axes in mcGillite, which has not been observed in mica, may be compared with that of silicon carbide polytypes. For the origin of such long-period superstructures in mcGillite, as Takeda & Ross (1975) proposed, an initial stage of crystal growth would play an important role because the formation of polytypes does not require a long-range interaction.

I would like to thank Professor G. Donnay who interested me in the problem of mcGillite and kindly provided the crystal. Financial support from NSF Grant DMR 8015785 is gratefully acknowledged. This research was also supported by the facility for High-Resolution Electron Microscopy, established with support from the NSF Regional Instrumentation Facilities Program (Grant CHE-7916098).

References

BAUER, L. H. & BERMAN, G. (1928). *Am. Mineral.* **13**, 341–348.

DONNAY, G., BETOURNAY, M. & HAMILL, G. (1980). *Can. Mineral.* **18**, 31–36.

IIJIMA, S. (1982). A**38**, 685–694.

IIJIMA, S. & BUSECK, P. R. (1978). *Acta Cryst.* A**34**, 709–719.

O'KEEFE, M. A., BUSECK, P. R. & IIJIMA, S. (1978). *Nature (London)*, **274**, 322–324.

TAKEDA, H. & ROSS, M. (1975). *Am. Mineral.* **60**, 1030–1040.

TAKÉUCHI, Y., KAWADA, I., IRIMAGIRI, S. & SADANAGA, R. (1969). *Mineral. J.* **5**, 450–467.

TAKÉUCHI, Y., KAWADA, I. & SADANAGA, R. (1963). *Acta Cryst.* **16**, A16.